Toward Pt-Free Anion-Exchange Membrane Fuel Cells: Fe−Sn Carbon Nitride−Graphene Core−Shell Electrocatalysts for the Oxygen Reduction Reaction

Enrico Negro,[†,‡,§] Antoine Bach Delpeuch,[†] Keti Vezzù,[†,§] Graeme Nawn,[†] Federico Bertasi,*[,†,‡] Alberto Ansaldo,[∥] Vittorio Pellegrini,[∥] Beata Dembinska,[⊥] Sylwia Zoladek,[⊥] Krzysztof Miecznikowski,[⊥] Iwona A. Rutkowska,[⊥] Magdalena Skunik-Nuckowska,[⊥] Pawel J. Kulesza,[⊥] Francesco Bonaccorso,*[,‡] and Vito Di Noto*[,†,§,#]

[†]Section of "Chemistry for the Technology" (ChemTec), Department of Industrial Engineering, University of Padova, in the Department of Chemical Sciences, Via Marzolo 1, I-35131 Padova (PD), Italy

[‡]Centro Studi di Economia e Tecnica dell'Energia ≪Giorgio Levi Cases≫, Via Marzolo 9, 35131 Padova (PD), Italy

[§]Consorzio Interuniversitario per la Scienza e la Tecnologia dei Materiali (INSTM)

[∥]stituto Italiano di Tecnologia, Graphene Labs, Via Morego 30, 16163 Genova (GE), Italy

[⊥]Faculty of Chemistry, University of Warsaw, Pastuera 1, 02-093 Warsaw, Poland

[#]CNR-ICMATE, Via Marzolo 1, I-35131 Padova (PD), Italy

Materials Science and Engineering Department, Universidad Carlos III de Madrid, Escuela Politécnica Superior, Av.de la Universidad, 30, 28911 Leganes, Spain

Ⓢ *Supporting Information*

ABSTRACT: We report on the development of two new *Pt-free* electrocatalysts (ECs) for the oxygen reduction reaction (ORR) process based on graphene nanoplatelets (GNPs). We designed the ECs with a *core−shell* morphology, where a GNP *core* support is covered by a carbon nitride (CN) *shell*. The proposed ECs present ORR active sites that are not associated with nanoparticles of metal/alloy/oxide but are instead based on Fe and Sn subnanometric clusters bound in *coordination nests* formed by carbon and nitrogen ligands of the CN *shell*.

The performance and reaction mechanism of the ECs in the ORR are evaluated in an alkaline medium by cyclic voltammetry with the thin-film rotating ring-disk approach and confirmed by measurements on gas-diffusion electrodes. The proposed GNP-supported ECs present an ORR overpotential of only ca. 70 mV higher with respect to a conventional Pt/C reference EC including a XC-72R carbon black support. These results make the reported ECs very promising for application in anion-exchange membrane fuel cells. Moreover, our methodology provides an example of a general synthesis protocol for the development of new *Pt-free* ECs for the ORR having ample room for further performance improvement beyond the state of the art.
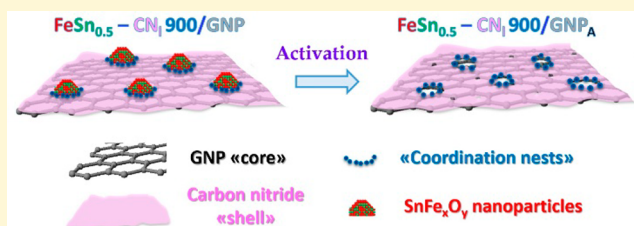
■ INTRODUCTION

The development of innovative, highly efficient, and environmentally friendly energy conversion devices is one of the major challenges faced today by both fundamental and applied research.[1] In this respect, fuel cells (FCs) show great promise owing to their high energy conversion efficiency (values of up to 60% or more are currently demonstrated)[2] and negligible emissions of pollutants and greenhouse gases.[3] Fuel cells based on polymeric ion-exchange membranes and operating at low temperatures, $T < 250$ °C (e.g., proton-exchange membrane fuel cells, PEMFCs, and high-temperature proton-exchange membrane fuel cells, HT-PEMFCs), attract considerable attention due to their very high power density (on the order of several hundreds of mW·cm^{-2} or more[4−6]) and easy construction in comparison with other types of FCs (e.g.,

molten carbonate fuel cells, MCFCs).[7−9] As an example, MCFCs require complex and bulky ancillary systems to recycle the CO$_2$ produced during operation; on the contrary, such systems are not needed in FCs based on polymeric ion-exchange membranes.[7−9] Massive research efforts have been dedicated to FCs,[10−12] with a particular reference to those based on polymeric ion-exchange membranes and operating at low temperatures. These systems typically adopt acid electrolytes (e.g., perfluorinated proton-exchange ionomers or polybenzimidazole imbibed with phosphoric acid).[8,13,14] Consequently, one of the critical bottlenecks in the operation
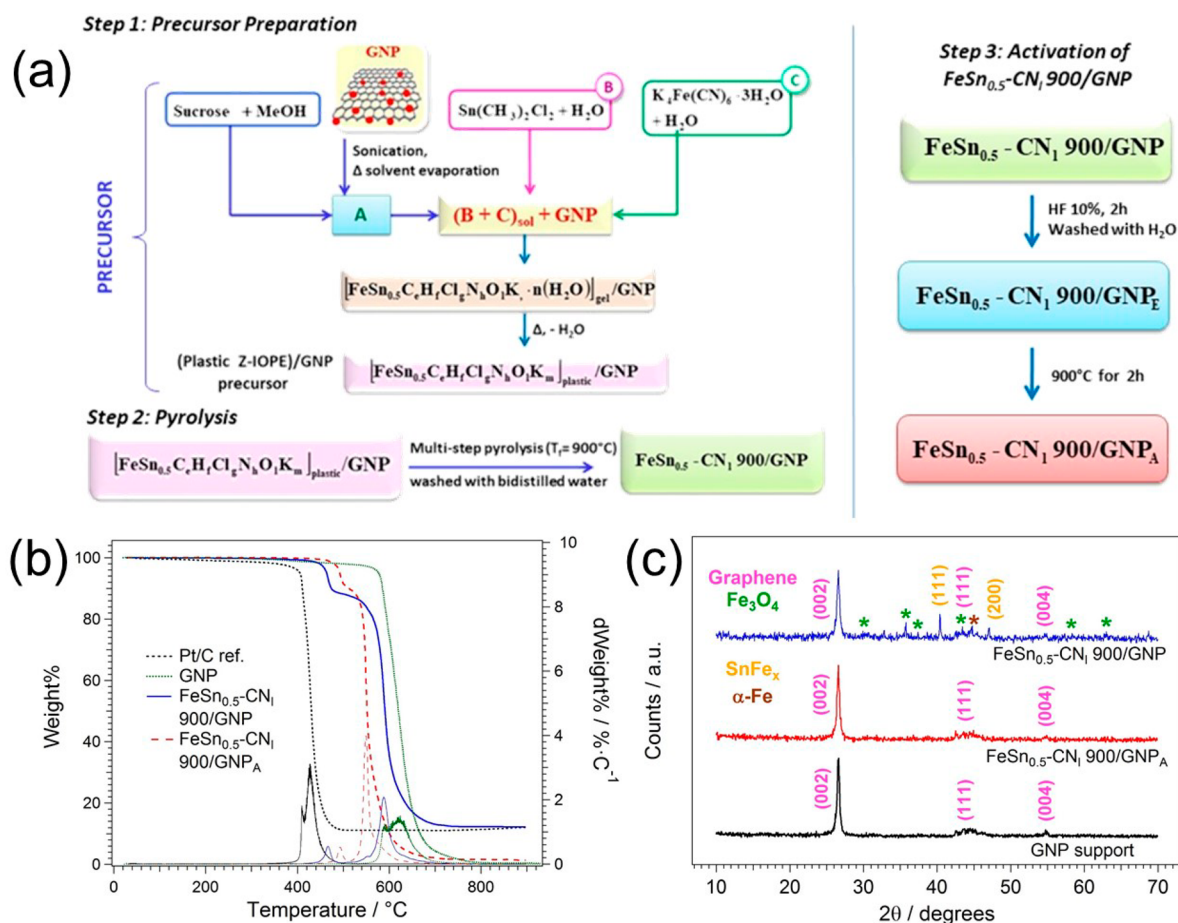
Figure 1. (a) Protocol for the preparation of the *core–shell* GNP-based ECs. *FeSn$_{0.5}$–CN$_l$ 900/GNP$_E$* is the intermediate product of the activation process, after the etching with HF and before the final pyrolysis at 900 °C. (b) HR-TGA profiles under an oxidizing atmosphere. (c) Powder XRD patterns of ECs and GNP support.

of these systems remains the sluggish kinetics of the oxygen reduction reaction (ORR) process at the cathode.[7,15−17] Here, the currently used cathodic electrocatalysts (ECs) are based on platinum-group metals (PGMs) for optimal operation in an acid medium, since *Pt-free* ECs still yield low performances under these conditions.[15,18] The abundance of PGMs in the Earth's crust is very low, on the order of 0.01 ppm.[19] Furthermore, the geographical distribution of PGM resources is very uneven, raising significant risks of supply bottlenecks.[20] This hampers the widespread rollout of these low-T FCs.[21] Recently, the aforementioned issues have been addressed by the development of anion-exchange membrane fuel cells (AEMFCs).[22,23] In these devices, the ORR takes place in an alkaline environment; accordingly, it occurs with a very different reaction mechanism in comparison with the acid medium.[24] Briefly, in the alkaline environment, the first adsorption of dioxygen and the first electron transfers are facilitated if compared with the same processes in the acid medium.[25] Consequently, in the alkaline medium, the ORR kinetics on PGM-free ECs is faster.[25] As of today, the performance level of PEMFCs is compatible with the standards required for practical applications;[26] typical power and current density values are on the order of ~700 mW·cm^{-2} and ~2000 mA·cm^{-2}, respectively.[6,27] Recently, AEMFCs mounting Pt-based ORR ECs and reaching a performance level comparable to the one of PEMFCs have been demonstrated.[28] Accordingly, it can be inferred that state-of-the-art hydroxide-exchange

membranes yield an ionic conductivity comparable to the one shown by the typical proton-exchange membranes adopted in PEMFCs, and no longer bottleneck AEMFC operation.[22] The literature reports AEMFCs that include Pd-based anodes and Ag-based cathodes exhibiting a power density of ~500 mW·cm^{-2};[29,30] other studies describe AEMFCs mounting Pt-based anodes and Ag-based cathodes yielding a power density of ~900 mW·cm^{-2} at a cell voltage of 0.6 V.[31] However, the performance of AEMFCs mounting ORR ECs that comprise neither PGMs (e.g., Pt, Pd) nor other precious metals such as silver is vastly inferior. In this case, power density values on the order of ~200 mW·cm^{-2} are described.[32] Finally, AEMFCs that mount PGM-free ECs at both the anode and the cathode demonstrate power density values on the order of ~50 mW·cm^{-2}.[29,33,34] Although these values are rather promising, they are still at least ~10−15 times lower in comparison with the one demonstrated by PGM-based ORR ECs. Thus, the development of advanced, highly performing PGM-free ORR ECs, coupled with a sufficient durability in an alkaline medium, is an objective of utmost importance[35] which is, however, far from being achieved.

Here, we design innovative *core–shell*, *Pt-free* carbon nitride (CN) ORR ECs based on Earth-abundant metals, which are anchored by covalent metal–carbon and metal–nitrogen bonds on the support. The proposed ECs consist of graphene nanoplatelet (GNP) *cores* covered by a thin CN matrix *shell* embedding active metal complex sites. Graphene nanoplatelet

cores are adopted with the aim to exploit (a) their negligible microporosity, to facilitate the mass transport of reactants (e.g., oxygen) and products (e.g., water) in the cathodic electrocatalytic layer of the AEMFC, and (b) their high electrical conductivity, to minimize the ohmic losses associated with the electron transport from the active sites to the external circuit.[36−40] The proposed graphene-based ECs are significantly different than those described in literature. In fact, the latter typically include oxide or nitride nanoparticles bearing the active sites to promote the ORR in an alkaline environment.[41,42] Furthermore, the ECs described in literature do not comprise a CN matrix *shell*.[43,44] Differently, in the proposed *core−shell Pt-free* ECs, the CN *shell* (i) is templated on the GNP *core* and (ii) coordinates the ORR active sites based on iron and tin. Thus, in the proposed *core−shell Pt-free* ECs, the active sites are not found on the surface of inorganic nanoparticles, forming a distinct component within the system. Iron is chosen for two reasons: (i) It gives rise to active sites where the first adsorption of dioxygen is facilitated; this affords fast ORR kinetics.[16,24] (ii) It easily forms strong metal−carbon coordination bonds with the CN matrix (the *shell*), improving the stability of the ORR active sites.[45] We propose the use of tin as a cocatalyst in the ORR process owing to (i) its high stability in the Sn−C bonds, which,[46] in a synergic way, stabilize the iron species in the active sites and (ii) its amphoteric character,[45] which facilitates the adsorption of dioxygen in the alkaline environment. The two ECs here proposed are labeled as $FeSn_{0.5}−CN_l$ 900/GNP and $FeSn_{0.5}−CN_l$ 900/GNP$_A$ in agreement with the widely accepted nomenclature.[16]

■ EXPERIMENTAL SECTION

Reagents. Dimethyltin dichloride, 95%, and potassium hexacyanoferrate (II) trihydrate, 98%, are purchased from ABCR and Sigma-Aldrich, respectively. Sucrose, molecular biology grade, is obtained from Alfa Aesar. Graphene nanoplatelets are purchased from ACS Material, LLC. Potassium hydroxide (KOH, 98.4 wt %), hydrofluoric acid (HF, 48 wt %), and perchloric acid (HClO₄, 67−72%) are bought from VWR International, Sigma-Aldrich and Fluka Analytical, respectively. Isopropanol (>99.8 wt %) and methyl alcohol (>99.8 wt %) are purchased from Sigma-Aldrich. EC-10 electrocatalyst is acquired from ElectroChem, Inc.; it has a nominal Pt loading of 10 wt % and is labeled *"Pt/C ref"* in the text. For reference gas-diffusion electrode (GDE) experiments, Pt(20%)/C from E-Tek is used. Vulcan XC-72R is supplied by Carbocrom s.r.l.; it is washed with H_2O_2 (10 vol %) prior to use. All of the reactants and solvents are used as received and do not undergo any additional purification procedure. Doubly distilled water is used in all of the experiments.

Synthesis of the Electrocatalysts.[16,47] 1 g of GNPs, 1 g of sucrose, and 2 mL of methanol are ground together for 9 h in an agate jar using a Retsch PM100 ball mill. The resulting product is treated with HF, 10 wt % for 2 h, and finally rinsed extensively with water, yielding the support *GNP*. A 355 mg portion of sucrose is dissolved in the minimum amount of methanol (i.e., ~40 mL); 355 mg of GNPs is subsequently added to the solution; the resulting dispersion is (i) homogenized for 2 min with a Bandelin Sonoplus HD 2200 probe sonicator, using ultrasonic impulses lasting 0.3 s each and separated by pauses 0.7 s long at a power rating of 20%, and (ii) transferred into a Teflon beaker. The dispersion is heated at ~60 °C in an oil bath and brought to a small volume (~1 mL) under vigorous stirring; the product is allowed to cool to room temperature. A 141 mg portion of potassium hexacyanoferrate (II) trihydrate is dissolved into the minimum amount of water (~1 mL); the resulting solution is added to the dispersion comprising the GNPs, which is then homogenized extensively with a probe sonicator adopting the same experimental parameters previously described. A 37 mg portion of dimethyltin dichloride is dissolved into the minimum amount of water (~1 mL),

yielding a solution which is finally added to the product above; the resulting dispersion is homogenized extensively with a probe sonicator (same parameters as above), vigorously stirred for a few minutes, allowed to rest for 24 h and finally dried in an oven for 120 °C. During these latter two processes, sol → gel and gel → plastic transitions occur,[48] giving rise to a (Plastic Z-IOPE)/GNP precursor (see Figure 1a). This latter product is placed into a quartz tube, where it undergoes a pyrolysis process comprising three steps, as follows: step 1, 150 °C, 7 h; step 2, 300 °C, 2 h; step 3, 900 °C, 2 h. The entire pyrolysis process is carried out under a dynamic vacuum of ~1 mbar. The product of the pyrolysis process is split into two aliquots. The first is treated three times with water, yielding the electrocatalyst labeled "$FeSn_{0.5}−CN_l$ 900/GNP". The second aliquot is treated with HF 10 wt % for 2 h, thoroughly washed with water, and finally transferred into a quartz tube, where a second 2 h pyrolysis step is carried out under a dynamic vacuum of ~1 mbar at 900 °C (activation process, "**A**"). This latter process yields the electrocatalyst indicated as "$FeSn_{0.5}−CN_l$ 900/GNP$_A$".

Instruments and Methods. The wt % of C, H, and N in the ECs is obtained by elemental analysis using a FISONS EA-1108 CHNS-O system. The assay of K, Fe, and Sn is evaluated by inductively coupled plasma atomic emission spectroscopy (ICP-AES). These measurements are carried out with a SPECTRO Acros spectrometer with EndOnPlasma torch. The digestion of the samples is performed as described elsewhere.[49] The only difference, with respect to the published procedure,[49] relies on the fact that the initial oxidation step is carried out at 850 °C for 2 h in a ventilated oven, instead of 600 °C for 3 h.[50] The emission lines are λ (Fe) = 259.940 nm, λ (K) = 766.490 nm, and λ (Sn) = 189.926 nm. Thermogravimetric studies at high resolution are carried out between 30 and 1000 °C by means of a TGA 295 analyzer (TA Instruments). The instrument sensitivity ranges from 0.1 to 2%·min⁻¹; the resolution is 1 μg. The heating ramp is adjusted on the basis of the first derivative of the weight loss, and can range from 50 to 0.001 °C·min⁻¹. The measurements are performed with an open Pt pan in an oxidizing atmosphere of dry air. Powder X-ray patterns are measured using an eXplorer diffractometer (GNR Instruments) mounting a monochromatized Cu Kα source in the 2θ range 10−70° with a 0.05° step and an integration time of 40 s. The MAUD software is used to analyze the data.[51] Transmission electron microscopy studies, both conventional and at high resolution, are executed with a Jeol 3010 apparatus mounting high-resolution pole pieces (0.17 nm point-to-point resolution) and a Gatan slowscan 794 CCD camera. All of the samples are prepared in agreement with a protocol described elsewhere.[52]

CV-TF-RRDE Measurements. The inks for the realization of the electrode are prepared as described elsewhere.[53] A 15 μL portion of each ink is pipetted onto the glassy carbon (GC) disk of a rotating ring-disk electrode (RRDE) tip. The latter is spun at ~700 rpm in the open air during drying to ensure that the final electrode film is uniform.[54] The loading of both $FeSn_{0.5}−CN_l$ 900/GNP and $FeSn_{0.5}−CN_l$ 900/GNP$_A$ on the GC disk of the RRDE tip is equal to 0.765 mg·cm⁻²; only in the case of the Pt/C ref, the Pt loading on the RRDE tip is 15 μg$_{Pt}$·cm⁻². The details of the electrochemical instrumentation and setup used to carry out the measurements are reported elsewhere.[50] Briefly, the RRDE used as the working electrode is mounted on a model 636 rotator (Pine Research Instrumentations); the collection efficiency of the Pt ring is equal to 0.39. The experiments are carried out with a Bio-Logic VSP multichannel potentiostat/galvanostat. In a first step, the electrode is dipped in an acid 0.1 M HClO₄ solution and cycled between E = 0.05 and 1.05 V vs reversible hydrogen electrode (RHE) under pure O₂ at a sweep rate of 100 mV·s⁻¹ as the RRDE tip is rotated at 1600 rpm. Cycling is interrupted as the voltammograms become stable. The same electrode is subsequently dipped in a 0.1 M KOH solution and cycled as described above between E = 0.05 and 1.05 V vs RHE until the voltammograms become stable; the final data are collected at ν = 20 mV·s⁻¹ as the rotator is spun at 1600 rpm. The ring electrode is kept at E = 1.2 V vs RHE for the detection of H_2O_2.[55] Hg/HgSO₄/K₂SO₄(sat.) and Hg/HgO/KOH(aq) (0.1 M) reference electrodes are used for the acid and alkaline environments and are placed in a separate compartment during the measurements. The

potential is reported in terms of the RHE scale, calibrated before each experiment in agreement with the procedure described in the literature.[56] The faradic ORR currents are obtained by subtracting from the voltammograms described above other voltammograms collected under exactly the same conditions but after saturating the KOH solution with N_2.[57] iR-correction is carried out adopting a procedure described in the literature.[58] The gases used to saturate the electrochemical cell (i.e., high-purity oxygen and nitrogen) are obtained from Air Liquide. The disk currents are normalized on the geometric area of the GC.

Galvanodynamic Measurements. The electrochemical activity of the ECs has also been tested with a homemade gas-diffusion electrode (GDE, geometric area of the active part, 0.916 cm^2) mounted into a Teflon holder (with provision for gas feeding from the back of the electrode) and containing a Pt ring as a current collector. The experiments have been performed with a CH Instruments (Austin, TX, USA) Model 920D workstation. A saturated calomel electrode is used as a reference electrode, and all potentials are expressed against the reversible hydrogen electrode (RHE). Platinum sheet serves as a counter electrode. The gas diffusion backing layer for the ECs is a carbon cloth (designation B, 30% wet proofing; BASF Fuel Cell Co). Inks have been prepared by grinding in an agate mortar the ECs materials together with a Vulcan XC-72R (Cabot, USA) at the 1 to 1 mass ratio, and 2-propanol (POCh, Poland) (1 mL/10 mg of the catalyst + Vulcan) and 5% Nafion-1100 resin solution (Sigma-Aldrich). The final content of Nafion is 10% relative to the weight of the EC + Vulcan. In the fabrication of GDEs, the mass ratios of Pt in the Pt/C ref vs the proposed ECs are the same as those in the CV-TF-RRDE approach, namely, on the level of 1 to 51. After sonication for 1 h, followed by mixing under magnetic stirring for 1 h, the appropriate volumes of inks have been dropped onto the carbon cloth, placed onto a hot-plate warmed up to a temperature of 353 K. Catalytic layers have been dried at 373 K to a constant weight followed by pressing them upon application of 2 kg·cm^{-2} for 30 s. The loading of the ECs is ~2 mg·cm^{-2}. The measured currents have been recalculated against exact masses of each catalyst (expressed as specific currents). The preconditioning protocol has been identical to that for CV-TF-RRDE measurements. After open circuit potential (OCP) stabilization in oxygen-saturated 1 M KOH, galvanodynamic curves have been collected at a current scan rate of 1 mA·s^{-1} and an oxygen flow of 50 mL·min^{-1}.

RESULTS AND DISCUSSION

Figure 1a shows the schematic of the experimental procedure adopted for the realization of the proposed ECs, i.e., by using GNPs covered with a tin and iron Z-IOPE (zeolitic–inorganic organic polymer electrolyte) precursor. The latter is produced by using a sucrose binder, followed by a multistep pyrolysis process.[25,47,59] It should be observed that $FeSn_{0.5}-CN_l$ 900/GNP$_A$ EC is obtained by carrying out an activation process ("A") on $FeSn_{0.5}-CN_l$ 900/GNP as described in the section "Synthesis of the Electrocatalysts".

The chemical composition of the ECs is obtained by ICP-AES and elemental analysis; it is shown in Table S1 of the Supporting Information and highlights the following:

(i) The hydrogen concentration in $FeSn_{0.5}-CN_l$ 900/GNP is lower than 0.2 wt %, witnessing a very high graphitization degree of the CN shell.[16]

(ii) The wt % of nitrogen in the CN shell is lower than ~3 wt %. Indeed, nitrogen is only found in the CN shell, which comprises ~10 wt % of the whole EC (see Figure 1b). Thus, the concentration of nitrogen in the CN shell is ~10 times that determined for the whole ECs with microanalysis. For this reason, since the nitrogen concentration is at most 0.29 wt % (see Table S1 of the Supporting Information), we can deduce that the

maximum weight % of nitrogen in the shell is ~3 wt %. Under these conditions, in agreement with literature results on similar CN systems, we can assume that the electrical conductivity of the CN matrix is high enough ($> \sim(1-2) \times 10^{-2}$ S·cm^{-1}) to prevent significant ohmic losses.[16]

(iii) Both iron and tin are detected in $FeSn_{0.5}-CN_l$ 900/GNP; in fact, the tin/iron molar ratio is 0.1, which is quite different from the value expected on the basis of the reagent stoichiometry (i.e., 0.5). This result indicates that tin is more easily eliminated than iron during the pyrolysis and washing processes performed during the preparation of $FeSn_{0.5}-CN_l$ 900/GNP. Finally, a nitrogen/iron molar ratio of 0.25 is indicative of a significant amount of iron atoms that are not directly involved in coordination by the nitrogen-ligand functionalities of the CN shell.

With respect to $FeSn_{0.5}-CN_l$ 900/GNP, in $FeSn_{0.5}-CN_l$ 900/GNP$_A$:

(i) A significant reduction of the wt % of hydrogen (from 0.19 to 0.09 wt %) and nitrogen (from 0.29 to 0.04 wt %) is observed. Accordingly, it is concluded that the graphitization degree of the CN shell is enhanced and the electrical conductivity of the material is sufficient for the intended application as an ORR EC.[16] Unfortunately, a widely accepted, "quantitative" definition of "graphitization degree" is not available. In general, the lower the amount of heteroatoms (e.g., hydrogen, nitrogen, oxygen, sulfur, and others) in a carbon-based material, the higher its "graphitization degree".

(ii) Tin- and iron-based species are decreased from 1.3 to 0.4 wt % and from 4.68 to 0.14 wt %, respectively. Thus, it is concluded that the activation process affects significantly the chemical composition of the pristine $FeSn_{0.5}-CN_l$ 900/GNP.

After the activation process, the tin/iron and nitrogen/iron molar ratios of $FeSn_{0.5}-CN_l$ 900/Gr$_A$ increase to 1.5 and 1.13, respectively (see Table S1 of the Supporting Information), revealing the following:

(i) ~97% of iron species, which are not bound by carbon and nitrogen coordination functionalities forming the coordination nests of the CN matrix (the shell), are eliminated.

(ii) ~25% of tin species are removed. Thus, with respect to iron, the activation process has a lower impact on tin species. This fact could be due to the presence of Sn as Sn(IV) in $FeSn_{0.5}-CN_l$ 900/GNP$_A$. In fact, on the basis of the preparation method and results reported elsewhere,[45] it is expected that the Sn species are present as Sn(IV), which is the most stable state of tin under ambient conditions.

The high-resolution thermogravimetric analysis (HR-TGA) profiles in an oxidizing atmosphere of both $FeSn_{0.5}-CN_l$ 900/GNP and $FeSn_{0.5}-CN_l$ 900/GNP$_A$ ECs exhibit two clearly distinguished thermal degradation events: I and II (see Figure 1b). I occurs at $T_I < 500$ °C and is ascribed to the combustion of the CN shell in agreement with results determined on ECs that include a CN matrix with a similar nitrogen composition.[49] II, which takes place in the temperature range 540 °C < T_{II} < 590 °C, is associated with the oxidation of the remaining GNP core. Essentially, the activation process (i) raises T_I, confirming

previous results on the higher graphitization degree of the CN *shell*,[25] and (ii) lowers T_{II}, due to the generation of an increased amount of defects in the GNP support *core*. The high-temperature residue of $FeSn_{0.5}-CN_l$ 900/GNP corresponds to M_xO_y species with M = Fe, Sn.[25] The HR-TGA analysis demonstrates that $FeSn_{0.5}-CN_l$ 900/GNP$_A$ exhibits a negligible high-temperature residue (ca. 1.5%) (see Figure 1b) due to the low amount of metals in this EC (iron, 0.14%; tin, 0.4%; see Table S1 of the Supporting Information). Therefore, with respect to the Pt/C reference (where T_I occurs at ∼426 °C), the thermal stability of both pristine ($T_I \approx$ 466 °C) and activated ECs ($T_I \approx$ 492 °C) under an oxidizing atmosphere is significantly improved. In fact, in state-of-the-art Pt/C ECs, the thermal degradation under an oxidizing atmosphere of carbon-based supports is promoted by the platinum nanoparticles.[60] On this basis, the proposed graphene-based platinum-free ECs are very stable likely for the lack of metal alloy nanoparticles that typically promote their thermal degradation in the presence of an oxidizing atmosphere.[60]

The powder X-ray patterns of the ECs, shown in Figure 1c, exhibit (i) a high-intensity and sharp peak at $2\theta \sim 26.6°$, (ii) a broad peak at $2\theta \sim 44.5°$, and (iii) a low-intensity peak at $2\theta \sim 54.8°$. These reflections are attributed respectively to the (002), (111), and (004) peaks of the GNP component of the samples (COD #9008569), with the $P6_3/mc$ space group.[61] X-ray diffraction results reveal that, in the ECs, along the [001] direction the graphene layers are still partially stacked with a significant stacking fault disorder. This nanomorphology is probably modulated by the CN *shell* wrapping the graphene support. The X-ray pattern of $FeSn_{0.5}-CN_l$ 900/GNP also shows peaks associated with three additional phases, i.e.: (i) magnetite, Fe_3O_4 (COD #9006247);[61] (ii) alloy nanoparticles comprising a random solid solution of tin and iron, indicated as $SnFe_{0.39}$ (COD #9012707);[61] and (iii) α-Fe (COD #1100108).[61] The presence of Fe_3O_4, $SnFe_x$, and α-Fe phases, which belong respectively to the Fd-$3m$, Fm-$3m$, and Im-$3m$ space groups,[61] is in agreement with the chemical composition of the ECs summarized in Table S1 of the Supporting Information. Structural information (i.e., abundance, cell parameters, and particle size) derived from the Rietveld analysis for $FeSn_{0.5}-CN_l$ 900/GNP is reported in Table S2 of the Supporting Information. The X-ray pattern of $FeSn_{0.5}-CN_l$ 900/GNP$_A$ reveals only peaks associated with the GNP component, demonstrating that the activation process removes almost completely the metal-based nanoparticles incorporated in the pristine $FeSn_{0.5}-CN_l$ 900/GNP. The morphology of $FeSn_{0.5}-CN_l$ 900/GNP and $FeSn_{0.5}-CN_l$ 900/GNP$_A$ is shown in Figure 2.

$FeSn_{0.5}-CN_l$ 900/GNP shows small ($d < 100$ nm) nanoparticles (mostly based on Fe_3O_4), which are embedded in a CN *shell* covering the GNP *core*. In particular, the sub-100 nm nanoparticles are encapsulated in a compact *onion-like* CN *shell* (highlighted in yellow in Figure 2c and e). The interplanar distance evidenced in the small nanoparticles (Figure 2e) corresponds to the d_{131} value of a typical Fe_3O_4 phase, confirming the identification of the latter in the powder X-ray pattern reported in Figure 1c. After the activation process, very few metal-based nanoparticles are observed in the *shell* of EC (see Figure 2b): the density of the metal-based nanoparticles in $FeSn_{0.5}-CN_l$ 900/GNP$_A$ is ∼40−45 nanoparticles·μm^{-2}, ca. one-third the value determined on $FeSn_{0.5}-CN_l$ 900/GNP. The activation process of the ECs gives rise to a cratered CN *shell* covering the GNP *core* (e.g., see the crater highlighted in
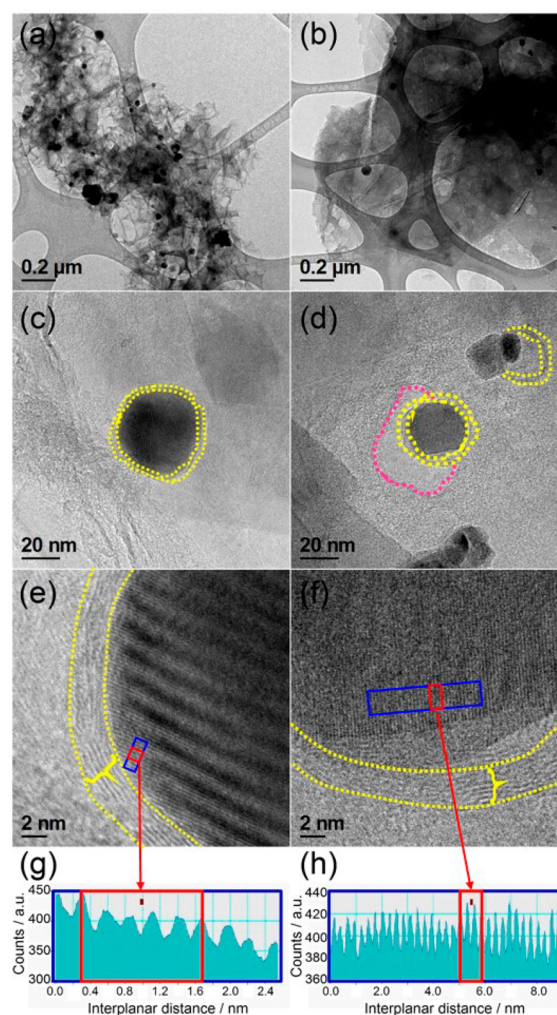

Figure 2. HR-TEM micrographs of (a, c, e) $FeSn_{0.5}-CN_l$ 900/GNP and (b, d, f) $FeSn_{0.5}-CN_l$ 900/GNP$_A$ at different magnifications. The interplanar distances d_{131} of the Fe_3O_4 phases of (g) $FeSn_{0.5}-CN_l$ 900/GNP and (h) $FeSn_{0.5}-CN_l$ 900/GNP$_A$ are shown.

purple in Figure 2d); the morphology of the CN *shell* is not altered. In few instances, the *onion-like* features of the CN shell matrix are still visible (see Figure 2d and f), and inhibit the etching of the sub-100 nm nanoparticles underneath.

The ORR performance of the ECs in the alkaline environment is investigated by cyclic voltammograms (see Figure 3a) and Tafel plots (see Figure 3b).[52]

The ORR performance, selectivity, and reaction mechanism of $FeSn_{0.5}-CN_l$ 900/GNP and $FeSn_{0.5}-CN_l$ 900/GNP$_A$ ECs are not influenced by the activation process. On these bases, it is inferred that (i) the active ORR sites of both ECs are similar; (ii) the sub-100 nm nanoparticles, that are mostly detected on $FeSn_{0.5}-CN_l$ 900/GNP only, play a negligible role in the ORR; and (iii) the ORR active sites are located on features present in both ECs, namely, the iron and tin species stabilized in the *coordination nests* of the CN *shell*. With respect to the Pt/C reference: (i) the ORR overpotential of both ECs here proposed is only ∼70 mV higher; (ii) the ORR mechanism is the same, as demonstrated by the Tafel slope (see Figure 3b);[24,62] and (iii) the selectivity determined as elsewhere reported[55] in the 4e-ORR pathway is lower, as indicated by the higher amount of H_2O_2 produced.
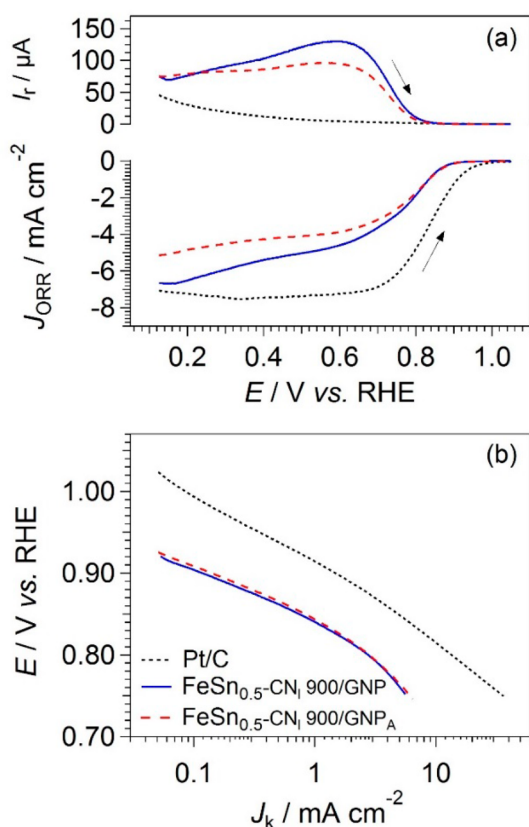
Figure 3. (a) CV-TF-RRDE anodic J_{ORR} and I_r profiles and (b) corresponding Tafel plots of the ECs in O_2-saturated 0.1 M KOH; ω = 1600 rpm; ν = 20 mV·s^{-1}; T = 298 K.

Overall, the ORR overpotential of both FeSn$_{0.5}$−CN$_l$ 900/GNP and FeSn$_{0.5}$−CN$_l$ 900/GNP$_A$ is already comparable with that exhibited by other *Pt-free* ECs including Fe as the *"active metal"*[16] and a variety of supports exhibiting different morphologies.[63,64] However, additional efforts are currently underway to further reduce this ORR overpotential and better exploit the potential of the proposed synthetic route. Some possibilities include: (i) the increase of the surface density of subnanometric metal clusters fixed on the surface of the CN *shell* and (ii) the modulation of the stoichiometric ratio between the metal atoms and the nitrogen species embedded in the CN shell.[25]

From the perspective of the electrochemical mechanism, the results reported in Figure 3 are rationalized admitting that during the ORR the first adsorption of dioxygen in the alkaline medium is followed by charge transfer occurring through an *outer-sphere* process.[24] A significant fraction of hydrogen peroxide, $X_{H_2O_2}$, is thus obtained (see Figure S3 of the Supporting Information; $X_{H_2O_2}$ values on the order of 45% at E = 0.5 V vs RHE are detected), which is readily expelled from the electrode layer on the RRDE disk and eventually detected at the ring electrode. These values are comparable with those reported in the literature for other similar ECs.[25,63] This evidence confirms that the proposed ECs exhibit a very low microporosity. In prospective, this is a very useful feature, as it facilitates the mass transport of reactants and products. This mitigates the concentration overpotentials at high current densities in the FCs mounting on the cathode the proposed ECs.[65] Indeed, if the proposed ECs had a high microporosity,

the hydrogen peroxide produced during the ORR would be trapped in the cavities of the EC, undergoing a further reduction to H_2O. This would allow extracting two more electrons from a single dioxygen molecule, boosting the energy conversion efficiency of the system at the expense of more severe concentration overpotentials in the final FC.

The galvanodynamic profiles determined on GDEs (Figure 4) show that half-cell potentials yielded by the Pt/C reference
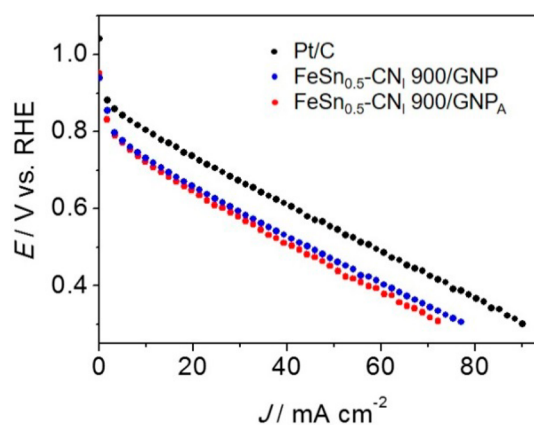

Figure 4. Galvanodynamic steady-state polarization responses for ORR recorded using GDEs in O_2-saturated 1 M KOH solution; catalyst loading: ~2 mg·cm^{-2}; O_2 flux = 50 mL·min^{-1}; T = 298 K.

are only 70−80 mV higher with respect to those obtained with the proposed ECs. Furthermore, the traces of FeSn$_{0.5}$−CN$_l$ 900/GNP and FeSn$_{0.5}$−CN$_l$ 900/GNP$_A$ ECs are almost coincident. In detail, the potential detected on the GDEs at a current density of 40 mA·cm^{-2} is equal to 0.53 and 0.51 V vs RHE for FeSn$_{0.5}$−CN$_l$ 900/GNP and FeSn$_{0.5}$−CN$_l$ 900/GNP$_A$ ECs, respectively. These results are in agreement with the outcome of CV-TF-RRDE experiments (see Figure 3a).

Accordingly, it is demonstrated that the proposed ECs are able to operate effectively both under almost ideal conditions (i.e., those achieved by the CV-TF-RRDE experimental setup[66]) and in an environment (i.e., a GDE) that closely mimics the cathodic electrode layer of a real AEMFC being affected by ohmic and concentration overpotentials. This result allows inferring that the proposed ECs have the potential to be successfully implemented in the fabrication of the cathodic electrocatalytic layer of an AEMFC. The development of ORR electrocatalysts able to operate without the introduction of parasitic overpotentials in the presence of methanol is an important objective of the research in the field of direct methanol fuel cells (DMFCs).[67,68] The tolerance of the proposed ECs toward methanol poisoning is gauged by recording the GDE polarization curves in electrolytes containing 1 M CH$_3$OH (see Figure S4 of the Supporting Information). Contrary to conventional Pt/C ECs reported in literature,[69,70] the performance in the ORR of the proposed ECs is largely unchanged, thus implying tolerance of the proposed *Pt-free, core−shell* GNP-based ECs to the presence of an organic fuel such as methanol.

■ **CONCLUSIONS**

Here, we design and synthesize *core−shell* ECs for the ORR process (FeSn$_{0.5}$−CN$_l$ 900/GNP), which includes metal-based nanoparticles embedded in a CN *shell* templated on graphene nanoplatelet *cores*. In addition, we propose an activation

process, which is suitable to improve the graphitization degree of the CN *shell* and removes most of the metal-based nanoparticles without a significant impact on the ORR performance, yielding the $FeSn_{0.5}-CN_l$ 900/GNP_A sample. The multistep synthetic approach exploited for the realization of the ECs is very general. This opens the door to a large number of further syntheses to obtain *Pt-free* ECs for the ORR with a well-controlled chemical composition, morphology, and structure, capable of operation at overpotentials less than 100 mV higher with respect to the one of Pt and with a high selectivity toward the four-electron reduction of dioxygen to water. Results reveal that the ORR active sites of the proposed ECs (i) are not located on the metal-based NPs detected in pristine $FeSn_{0.5}-CN_l$ 900/GNP (i.e., Fe_3O_4, $SnFe_x$, and α-Fe) and (ii) present as subnanometric metal clusters fixed on the surface of the CN *shell*, where they are stabilized by *coordination nests*. These latter are formed by aggregates of carbon and nitrogen ligands provided by the CN matrix. Accordingly, these subnanometric metal clusters are very stable. Indeed, they are not removed during the activation process and bestow to $FeSn_{0.5}-CN_l$ 900/GNP and $FeSn_{0.5}-CN_l$ 900/GNP_A a remarkable ORR activity. In fact, the ORR overpotential of the proposed ECs is only ~70 mV higher than that of the Pt/C ref despite the very low metal concentration (lower than 6 wt %) and total absence of PGMs. Finally, it is shown that the proposed ECs are (i) highly tolerant to methanol poisoning and (ii) able to effectively operate also in a gas-diffusion electrode setup, where the ORR performance is affected by charge and mass transport issues similar to those encountered at the cathodic electrocatalytic layer of a single AEMFC. This is a crucial result highlighting the feasibility of the proposed ECs to be implemented in a real device. Still, it is pointed out that the implementation of this type of state-of-the-art *Pt-free* ORR ECs in AEMFCs, that comprises neither PGMs nor precious metals such as Ag, is hindered by significant charge and mass transport issues typically arising from a nonoptimized porosity.[32] Consequently, the performance of the corresponding AEMFCs is still significantly inferior to that of AEMFCs mounting conventional Pt/C electrocatalysts.[29] On these bases, further research efforts need to be devoted to the optimization of the morphology and of the electrochemical performance of this family of *Pt-free* carbon nitride−graphene *core−shell* ECs, to fully realize their potential at the cathode of advanced AEMFCs.

■ ASSOCIATED CONTENT

Ⓢ Supporting Information

The Supporting Information is available free of charge on the ACS Publications website at DOI: 10.1021/acs.chemmater.7b05323.

> Chemical composition of the ECs; structural information derived from the Rietveld analysis of $FeSn_{0.5}-CN_l$ 900/GNP; results of the powder XRD pattern decomposition by the Rietveld procedure of the $FeSn_{0.5}-CN_l$ 900/GNP EC; cyclic voltammograms of $FeSn_{0.5}-CN_l$ 900/GNP, $FeSn_{0.5}-CN_l$ 900/GNP_A, and Pt/C ref in N_2-saturated 0.1 M KOH; evolution of the selectivity toward production of H_2O_2 against the potential of the investigated ECs in O_2-saturated 0.1 M KOH; galvanodynamic steady-state polarization responses for ORR using GDE in O_2-saturated 1 M KOH and 1 M KOH + 1 M CH_3OH (PDF)

■ AUTHOR INFORMATION

Corresponding Authors

*E-mail: (V.D.N.) vito.dinoto@unipd.it;
*E-mail: (F.B.) federico.bertasi@unipd.it;
*E-mail: (F. B.) francesco.bonaccorso@iit.it.

ORCID Ⓞ

Keti Vezzù: 0000-0003-4156-7479
Alberto Ansaldo: 0000-0002-3493-4157
Krzysztof Miecznikowski: 0000-0001-7401-5844
Francesco Bonaccorso: 0000-0001-7238-9420
Vito Di Noto: 0000-0002-8030-6979

■ REFERENCES

(1) Poizot, P.; Dolhem, F. Clean energy new deal for a sustainable world: From non-CO_2 generating energy sources to greener electrochemical storage devices. *Energy Environ. Sci.* **2011**, *4*, 2003−2019.

(2) Wang, Y.; Chen, K. S.; Mishler, J.; Cho, S. C.; Adroher, X. C. A review of polymer electrolyte membrane fuel cells: Technology, applications, and needs on fundamental research. *Appl. Energy* **2011**, *88*, 981−1007.

(3) O'Hayre, R.; Cha, S. W.; Colella, W.; Printz, F. B. *Fuel Cell Fundamentals*; John Wiley & Sons: Hoboken, NJ, 2006.

(4) Wei, Z.; Su, K.; Sui, S.; He, A.; Du, S. High performance polymer electrolyte membrane fuel cells (PEMFCs) with gradient Pt nanowire cathodes prepared by decal transfer method. *Int. J. Hydrogen Energy* **2015**, *40*, 3068−3074.

(5) Rosli, R. E.; Sulong, A. B.; Daud, W. R. W.; Zulkifley, M. A.; Husaini, T.; Rosli, M. I.; Majlan, E. H.; Haque, M. A. A review of high-temperature proton exchange membrane fuel cell (HT-PEMFC) system. *Int. J. Hydrogen Energy* **2017**, *42*, 9293−9314.

(6) Li, Z. F.; Xin, L.; Yang, F.; Liu, Y.; Zhang, H.; Stanciu, L.; Xie, J. Hierarchical polybenzimidazole-grafted graphene hybrids as supports for Pt nanoparticle catalysts with excellent PEMFC performance. *Nano Energy* **2015**, *16*, 281−292.

(7) Shao, Y.; Yin, G.; Wang, Z.; Gao, Y. Proton exchange membrane fuel cell from low temperature to high temperature: Material challenges. *J. Power Sources* **2007**, *167*, 235−242.

(8) Di Noto, V.; Zawodzinski, T. A.; Herring, A. M.; Giffin, G. A.; Negro, E.; Lavina, S. Polymer electrolytes for a hydrogen economy. *Int. J. Hydrogen Energy* **2012**, *37*, 6120−6131.

(9) Farooque, M.; Ghezel-Ayagh, H. In *Handbook of Fuel Cells - Fundamentals, Technology and Applications*; Vielstich, V., Lamm, A.,

Gasteiger, H. A., Eds.; John Wiley & Sons: Chichester, U.K., 2003; Vol. 3, pp 942−968.

(10) ElectroCat - Electrocatalysis Consortium, http://www.electrocat.org/, retrieved on Dec 20, 2017.

(11) Fuel Cell Technologies Office Multi-Year Research, Development, and Demonstration Plan, https://energy.gov/eere/fuelcells/downloads/fuel-cell-technologies-office-multi-year-research-development-and-22, retrieved on Dec 20, 2017.

(12) Fuel Cell and Hydrogen Joint Undertaking, http://www.fch.europa.eu/, retrieved on Dec 20, 2017.

(13) Kraytsberg, A.; Ein-Eli, Y. Review of advanced materials for proton exchange membrane fuel cells. Energy Fuels 2014, 28, 7303−7330.

(14) Kim, D. J.; Jo, M. J.; Nam, S. Y. A review of polymer-nanocomposite electrolyte membranes for fuel cell application. J. Ind. Eng. Chem. 2015, 21, 36−52.

(15) Katsounaros, I.; Cherevko, S.; Zeradjanin, A. R.; Mayrhofer, K. J. J. Oxygen electrochemistry as a cornerstone for sustainable energy conversion. Angew. Chem., Int. Ed. 2014, 53, 102−121.

(16) Di Noto, V.; Negro, E.; Vezzù, K.; Bertasi, F.; Nawn, G. Origins, Developments and Perspectives of Carbon Nitride-Based Electrocatalysts for Application in Low-Temperature FCs. Electrochem. Soc. Interface 2015, 24, 59−64.

(17) Li, Q.; He, R.; Jensen, J. O.; Bjerrum, N. J. Approaches and Recent Development of Polymer Electrolyte Membranes for Fuel Cells Operating above 100 °C. Chem. Mater. 2003, 15, 4896−4915.

(18) Guo, S.; Zhang, S.; Sun, S. Tuning nanoparticle catalysis for the oxygen reduction reaction. Angew. Chem., Int. Ed. 2013, 52, 8526−8544.

(19) Greenwood, N. N.; Earnshaw, A. Chemistry of the Elements; Butterworth-Heinemann Ltd: Oxford, U.K., 1984.

(20) Moss, R. L.; Tzimas, E.; Willis, P.; Arendorf, J.; Tercero Espinoza, L. Critical Metals in the Path towards the Decarbonisation of the EU Energy Sector - Assessing Rare Metals as Supply-Chain Bottlenecks in Low-Carbon Energy Technologies; Publications Office of the European Union: Luxembourg, 2013.

(21) 2011 Technology Map of the European Strategic Energy Technology Plan (SET-Plan) - Technology Descriptions; Brussels, 2011.

(22) Varcoe, J. R.; Atanassov, P.; Dekel, D. R.; Herring, A. M.; Hickner, M. A.; Kohl, P. A.; Kucernak, A. R.; Mustain, W. E.; Nijmeijer, K.; Scott, K.; Xu, T.; Zhuang, L. Anion-exchange membranes in electrochemical energy systems. Energy Environ. Sci. 2014, 7, 3135−3191.

(23) Merle, G.; Wessling, M.; Nijmeijer, K. Anion exchange membranes for alkaline fuel cells: A review. J. Membr. Sci. 2011, 377, 1−35.

(24) Ramaswamy, N.; Mukerjee, S. Influence of inner- and outer-sphere electron transfer mechanisms during electrocatalysis of oxygen reduction in alkaline media. J. Phys. Chem. C 2011, 115, 18015−18026.

(25) Vezzù, K.; Bach Delpeuch, A.; Negro, E.; Polizzi, S.; Nawn, G.; Bertasi, F.; Pagot, G.; Artyushkova, K.; Atanassov, P.; Di Noto, V. Fe-carbon nitride Core-shell electrocatalysts for the oxygen reduction reaction. Electrochim. Acta 2016, 222, 1778−1791.

(26) 3.4 Fuel Cells, 2016, https://energy.gov/sites/prod/files/2017/05/f34/fcto_myrdd_fuel_cells.pdf, retrieved on Dec 20, 2017.

(27) Tian, Z. Q.; Lim, S. H.; Poh, C. K.; Tang, Z.; Xia, Z.; Luo, Z.; Shen, P. K.; Chua, D.; Feng, Y. P.; Shen, Z.; Lin, J. A Highly Order-Structured Membrane Electrode Assembly with Vertically Aligned Carbon Nanotubes for Ultra-Low Pt Loading PEM Fuel Cells. Adv. Energy Mater. 2011, 1, 1205−1214.

(28) Ponce-González, J.; Whelligan, D. K.; Wang, L.; Bance-Soualhi, R.; Wang, Y.; Peng, Y.; Peng, H.; Apperley, D. C.; Sarode, H. N.; Pandey, T. P.; Divekar, A. G.; Seifert, S.; Herring, A. M.; Zhuang, L.; Varcoe, J. R. High performance aliphatic-heterocyclic benzyl-quaternary ammonium radiation-grafted anion-exchange membranes. Energy Environ. Sci. 2016, 9, 3724−3735.

(29) Dekel, D. R. Review of cell performance in anion exchange membrane fuel cells. J. Power Sources 2018, 375, 158−169.

(30) Miller, H. A.; Lavacchi, A.; Vizza, F.; Marelli, M.; Di Benedetto, F.; D'Acapito, F.; Paska, Y.; Page, M.; Dekel, D. R. A Pd/C-CeO2 Anode Catalyst for High-Performance Platinum-Free Anion Exchange Membrane Fuel Cells. Angew. Chem. 2016, 128, 6108−6111.

(31) Gottesfeld, S.; Dekel, D. R.; Page, M.; Bae, C.; Yan, Y.; Zelenay, P.; Kim, Y. S. Anion exchange membrane fuel cells: Current status and remaining challenges. J. Power Sources 2018, 375, 170−184.

(32) Serov, A.; Zenyuk, I. V.; Arges, C. G.; Chatenet, M. Hot topics in alkaline exchange membrane fuel cells. J. Power Sources 2018, 375, 149−157.

(33) Dhavale, V. M.; Singh, S. K.; Nadeema, A.; Gaikwad, S. S.; Kurungot, S. Nanocrystalline Fe-Fe2O3 particle-deposited N-doped graphene as an activity-modulated Pt-free electrocatalyst for oxygen reduction reaction. Nanoscale 2015, 7, 20117−20125.

(34) Unni, S. M.; Bhange, S. N.; Illathvalappil, R.; Mutneja, N.; Patil, K. R.; Kurungot, S. Nitrogen-induced surface area and conductivity modulation of carbon nanohorn and its function as an efficient metal-free oxygen reduction electrocatalyst for anion-exchange membrane fuel cells. Small 2015, 11, 352−362.

(35) Poynton, S. D.; Kizewski, J. P.; Slade, R. C. T.; Varcoe, J. R. Novel electrolyte membranes and non-Pt catalysts for low temperature fuel cells. Solid State Ionics 2010, 181, 219−222.

(36) Huang, X.; Qi, X.; Boey, F.; Zhang, H. Graphene-based composites. Chem. Soc. Rev. 2012, 41, 666−686.

(37) Quesnel, E.; Roux, F.; Emieux, F.; Faucherand, P.; Kymakis, E.; Volonakis, G.; Giustino, F.; Martín-García, B.; Moreels, I.; Gürsel, S. A.; Yurtcan, A. B.; Di Noto, V.; Talyzin, A.; Baburin, I.; Tranca, D.; Seifert, G.; Crema, L.; Speranza, G.; Tozzini, V.; Bondavalli, P.; Pognon, G.; Botas, C.; Carriazo, D.; Singh, G.; Rojo, T.; Kim, G.; Yu, W.; Grey, C. P.; Pellegrini, V. Graphene-based technologies for energy applications, challenges and perspectives. 2D Mater. 2015, 2, 030204.

(38) Geim, A. K.; Novoselov, K. S. The rise of graphene. Nat. Mater. 2007, 6, 183−191.

(39) Ferrari, A. C.; Bonaccorso, F.; Fal'ko, V.; Novoselov, K. S.; Roche, S.; Bøggild, P.; Borini, S.; Koppens, F. H. L.; Palermo, V.; Pugno, N.; Garrido, J. A.; Sordan, R.; Bianco, A.; Ballerini, L.; Prato, M.; Lidorikis, E.; Kivioja, J.; Marinelli, C.; Ryhänen, T.; Morpurgo, A.; Coleman, J. N.; Nicolosi, V.; Colombo, L.; Fert, A.; Garcia-Hernandez, M.; Bachtold, A.; Schneider, G. F.; Guinea, F.; Dekker, C.; Barbone, M.; Sun, Z.; Galiotis, C.; Grigorenko, A. N.; Konstantatos, G.; Kis, A.; Katsnelson, M.; Vandersypen, L.; Loiseau, A.; Morandi, V.; Neumaier, D.; Treossi, E.; Pellegrini, V.; Polini, M.; Tredicucci, A.; Williams, G. M.; Hee Hong, B.; Ahn, J. H.; Min Kim, J.; Zirath, H.; Van Wees, B. J.; Van Der Zant, H.; Occhipinti, L.; Di Matteo, A.; Kinloch, I. A.; Seyller, T.; Quesnel, E.; Feng, X.; Teo, K.; Rupesinghe, N.; Hakonen, P.; Neil, S. R. T.; Tannock, Q.; Löfwander, T.; Kinaret, J. Science and technology roadmap for graphene, related two-dimensional crystals, and hybrid systems. Nanoscale 2015, 7, 4598−4810.

(40) Bonaccorso, F.; Colombo, L.; Yu, G.; Stoller, M.; Tozzini, V.; Ferrari, A. C.; Ruoff, R. S.; Pellegrini, V. Graphene, related two-dimensional crystals, and hybrid systems for energy conversion and storage. Science 2015, 347, 1246501.

(41) Zhao, Q.; Li, Y.; Huang, K.; Wang, Q.; Zhang, J. Hierarchical hybrid of Ni3N/N-doped reduced graphene oxide nanocomposite as a noble metal free catalyst for oxygen reduction reaction. Appl. Surf. Sci. 2017, 400, 245−253.

(42) Hong, W.; Li, L.; Xue, R.; Xu, X.; Wang, H.; Zhou, J.; Zhao, H.; Song, Y.; Liu, Y.; Gao, J. One-pot hydrothermal synthesis of Zinc ferrite/reduced graphene oxide as an efficient electrocatalyst for oxygen reduction reaction. J. Colloid Interface Sci. 2017, 485, 175−182.

(43) Lv, R.; Wang, H.; Yu, H.; Peng, F. Controllable Preparation of Holey Graphene and Electrocatalytic Performance for Oxygen Reduction Reaction. Electrochim. Acta 2017, 228, 203−213.

(44) Pascone, P.-A.; Meunier, J.-L.; Berk, D. Influence of iron on structure and catalyst activity of nitrogen-functionalized graphene nanoflakes. Mater. Today Comm 2016, 9, 54−59.

(45) Cotton, F. A.; Wilkinson, G.; Murillo, C. A.; Bochmann, M. Advanced Inorganic Chemistry; John Wiley And Sons: New York, 1999.

(46) Elschenbroich, C.; Salzer, A. *Organometallics - A concise introduction*, 2nd ed.; VCH Verlagsgesellschaft: Weinheim, Germany, 1992.

(47) Di Noto, V.; Negro, E.; Bertasi, F.; Nawn, G.; Vezzù, K.; Toncelli, L.; Zeggio, S.; Bassetto, F. Electrocatalysts based on a carbon nitride matrix, 2015. Italian Patent Application #102015000055603. Priority date: Sept 28, 2015.

(48) Di Noto, V. Zeolitic Inorganic−Organic Polymer Electrolyte Based on Oligo(ethylene glycol) 600 K_2PdCl_4 and $K_3Co(CN)_6$. *J. Phys. Chem. B* **2000**, *104*, 10116−10125.

(49) Di Noto, V.; Negro, E.; Gliubizzi, R.; Gross, S.; Maccato, C.; Pace, G. Pt and Ni Carbon Nitride electrocatalysts for the oxygen reduction reaction. *J. Electrochem. Soc.* **2007**, *154*, B745−B756.

(50) Di Noto, V.; Negro, E. Pt-Fe and Pt-Ni carbon nitride-based ″Core-Shell″ ORR electrocatalysts for application Polymer Electrolyte Membrane Fuel Cells. *Fuel Cells* **2010**, *10*, 234−244.

(51) Lutterotti, L. *Materials Analysis Using Diffraction - MAUD*, v 2.33. http://maud.radiographema.com/, 2010.

(52) Negro, E.; Vezzù, K.; Bertasi, F.; Schiavuta, P.; Toniolo, L.; Polizzi, S.; Di Noto, V. Interplay between Nitrogen Concentration, Structure, Morphology, and Electrochemical Performance of PdCoNi ″Core-Shell″ Carbon Nitride Electrocatalysts for the Oxygen Reduction Reaction. *ChemElectroChem* **2014**, *1*, 1359−1369.

(53) Di Noto, V.; Negro, E.; Gliubizzi, R.; Lavina, S.; Pace, G.; Gross, S.; Maccato, C. A Pt-Fe Carbon Nitride Nano-electrocatalyst for Polymer Electrolyte Membrane Fuel Cells and Direct-Methanol Fuel Cells: Synthesis, Characterization and Electrochemical Studies. *Adv. Funct. Mater.* **2007**, *17*, 3626−3638.

(54) Garsany, Y.; Baturina, O. A.; Swider-Lyons, K. E.; Kocha, S. S. Experimental methods for quantifying the activity of platinum electrocatalysts for the oxygen reduction reaction. *Anal. Chem.* **2010**, *82*, 6321−6328.

(55) Schmidt, T. J.; Paulus, U. A.; Gasteiger, H. A.; Behm, R. J. The oxygen reduction reaction on a Pt/carbon fuel cell catalyst in the presence of chloride anions. *J. Electroanal. Chem.* **2001**, *508*, 41−47.

(56) Gasteiger, H. A.; Kocha, S. S.; Sompalli, B.; Wagner, F. T. Activity benchmarks and requirements for Pt, Pt-alloy, and non-Pt oxygen reduction catalysts for PEMFCs. *Appl. Catal., B* **2005**, *56*, 9−35.

(57) Wang, J. X.; Uribe, F. A.; Springer, T. E.; Zhang, J.; Adzic, R. R. Intrinsic kinetic equation for oxygen reduction reaction in acidic media: The double Tafel slope and fuel cell applications. *Faraday Discuss.* **2009**, *140*, 347−362.

(58) Van Der Vliet, D.; Strmcnik, D. S.; Wang, C.; Stamenkovic, V. R.; Markovic, N. M.; Koper, M. T. M. On the importance of correcting for the uncompensated Ohmic resistance in model experiments of the Oxygen Reduction Reaction. *J. Electroanal. Chem.* **2010**, *647*, 29−34.

(59) Diodati, S.; Negro, E.; Vezzù, K.; Di Noto, V.; Gross, S. Oxygen reduction reaction and X-ray photoelectron spectroscopy character-isation of carbon nitride-supported bimetallic electrocatalysts. *Electrochim. Acta* **2016**, *215*, 398−409.

(60) Linse, N.; Gubler, L.; Scherer, G. G.; Wokaun, A. The effect of platinum on carbon corrosion behavior in polymer electrolyte fuel cells. *Electrochim. Acta* **2011**, *56*, 7541−7549.

(61) Crystallography Open Database, http://www.crystallography.net/, retrieved on Oct 12, 2017.

(62) Negro, E.; Polizzi, S.; Vezzù, K.; Toniolo, L.; Cavinato, G.; Di Noto, V. Interplay between morphology and electrochemical perform-ance of ″core-shell″ electrocatalysts for oxygen reduction reaction based on a PtNi$_x$ carbon nitride ″shell″ and a pyrolyzed polyketone nanoball ″core″. *Int. J. Hydrogen Energy* **2014**, *39*, 2828−2841.

(63) Guo, Q.; Zhao, D.; Liu, S.; Chen, S.; Hanif, M.; Hou, H. Free-standing nitrogen-doped carbon nanotubes at electrospun carbon nanofibers composite as an efficient electrocatalyst for oxygen reduction. *Electrochim. Acta* **2014**, *138*, 318−324.

(64) Liu, C.; Wang, J.; Li, J.; Luo, R.; Sun, X.; Shen, J.; Han, W.; Wang, L. Fe/N decorated mulberry-like hollow mesoporous carbon fibers as efficient electrocatalysts for oxygen reduction reaction. *Carbon* **2017**, *114*, 706−716.

(65) Di Noto, V.; Negro, E.; Polizzi, S.; Vezzù, K.; Toniolo, L.; Cavinato, G. Synthesis, studies and fuel cell performance of ″core-shell″ electrocatalysts for oxygen reduction reaction based on a PtNi$_x$ carbon nitride ″shell″ and a pyrolyzed polyketone nanoball ″core″. *Int. J. Hydrogen Energy* **2014**, *39*, 2812−2827.

(66) Schmidt, T. J.; Gasteiger, H. A. In *Handbook of Fuel Cells - Fundamentals, Technology and Applications*; Vielstich, V., Lamm, A., Gasteiger, H. A., Eds.; John Wiley & Sons: Chichester, U.K., 2003; Vol. 2, pp 316−333.

(67) Feng, Y.; Alonso-Vante, N. Nonprecious metal catalysts for the molecular oxygen-reduction reaction. *Phys. Status Solidi B* **2008**, *245*, 1792−1806.

(68) Wee, J. H.; Lee, K. Y. Overview of the development of CO-tolerant anode electrocatalysts for proton-exchange membrane fuel cells. *J. Power Sources* **2006**, *157*, 128−135.

(69) Jusys, Z.; Behm, R. J. Simultaneous oxygen reduction and methanol oxidation on a carbon-supported Pt catalyst and mixed potential formation-revisited. *Electrochim. Acta* **2004**, *49*, 3891−3900.

(70) Yang, H.; Alonso-Vante, N.; Lamy, C.; Akins, D. L. High methanol tolerance of carbon-supported Pt-Cr alloy nanoparticle electrocatalysts for oxygen reduction. *J. Electrochem. Soc.* **2005**, *152*, A704−A709.